Regioregularity Effects in Poly(3-hexylthiophene):PCBM-Based Solar Cells Incorporating Acid-Doped Polyaniline Nanotubes as an Interfacial Layer

Yu-Kai Han,[*,z] **Yi-Jang Lee, and Pei-Chen Huang**

Department of Chemical and Materials Engineering, National Kaohsiung University of Applied Sciences, Kaohsiung 807, Taiwan

We adopted the FeCl$_3$ and Grignard metathesis (McCullough) methods to synthesize three poly(3-hexylthiophene)s (P3HTs) exhibiting different degrees of regioregularity and then blended them with [6,6]-phenyl-C$_{61}$-butyric acid methyl ester (PCBM) to obtain bulk heterojunction phases on the top of an acid-doped polyaniline nanotube (a-PANINT) interfacial layer. From integration of ^{1}H NMR spectra, we determined that the three P3HTs had head-to-tail coupling contents of 67, 81, and 96%, respectively. The photovoltaic (PV) performance of P3HT:PCBM-based devices fabricated without the a-PANINT interfacial layer increased as the regioregularity of the P3HT increased. The presence of the a-PANINT interfacial layer resulted in improved PV performances of the P3HT:PCBM-based devices. This improvement in the PV performance resulted from the highly conductive, controlled one-dimensional tubular nanoscale morphology of the annealed a-PANINT interfacial layer, which mediated the efficient migration of photogenerated holes to the buffer layer and suppressed exciton recombination.
© 2009 The Electrochemical Society. [DOI: 10.1149/1.3071425] All rights reserved.

Organic conjugated polymers have drawn much attention in recent years because of their promising applications in electrochromics,[1] biosensors,[2] electrochemical supercapacitors,[3] anticorrosion materials,[4] polymer thin-film transistors,[5] polymer light-emitting diodes,[6] polymer photodetectors, and polymer solar cells.[7-11] Soluble polythiophene derivatives are the most promising and frequently investigated conjugated systems because of their synthetic availability, stability in various redox states, widespread processability, and tunable electronic properties.[12]

Poly(3-hexylthiophene) (P3HT) is at present one of the most useful electron-donor conjugated polymers for the preparation of bulk heterojunction (BHJ) polymer solar cells because of its high carrier mobility, thermal stability, and compatibility with solution processing. The electrical properties of this conjugated polymer are strongly dependent on its conformation and microstructure. The effects of the molecular weight,[13] polydispersity, and regioregularity[14] on the morphology and charge-transport phenomena of conjugated polymer materials have been discussed extensively.[10-12] P3HT by itself exhibits large mesostructural variations, depending on its molecular weight, casting solvent, and annealing treatment; these changes can affect its charge mobility.[15] The photoresponse of low-molecular-weight P3HT (weight-average molecular weight: M_w < 4000 g mol^{-1}) is limited by the confinement of the conjugation length, which is generally accepted to be greater than, but not far from, 20 units.[16] This value is increased as a result of solid-state effects. P3HT having a value of M_w of ca. 10,000 g mol^{-1} forms crystalline nanorods and exhibits low charge mobilities (μ) because of the poor long-range interconnectivity of the polymer chains. P3HT having an even higher molecular weight (M_w = ca. 30,000 g mol^{-1}) displays a completely different structure [one based on crystalline, interwoven fibrils connected over long distances (ca. 500 nm)] that leads to improved values of μ.[15]

Many methods for synthesizing regioregular poly(alkylthiophene)s (PATs) of various molecular weights have been published during the last few decades.[10-14] The photovoltaic (PV) performance of these conjugated polymers is highly dependent on their modes of π-π stacking. Regiorandom and highly regioregular PATs[17] can be obtained using the coupling methods developed by Sugimoto et al.,[18] Tamao et al.,[19,20] Yamamoto et al.,[21-24] Stille,[25] Kodama et al.,[26] Chen and Rieke,[27,28] Chen et al.,[29] Wu et al.,[31] McCullough et al.,[32] and Loewe et al.[33] Using Sugimoto et al.'s method, the monomer is treated with ferric chloride (FeCl$_3$), which oxidizes the

3-alkylthiophene monomer to produce radical cations having spin density located predominantly on the 2 and 5 positions of the thiophene ring; coupling of these radical actions produces polymers[34-36] having reasonably high molecular weights, but with broad polydispersity (PDI), which can lead to undesirable properties. Performing the reactions at lower temperatures or using vanadium-based oxidants can minimize the extent of these defects.

The Stille cross coupling and Rieke methods both lead to regioregular polymers. The Rieke method involves the reaction of 3-alkyl-2,5-dibromo-thiophene with activated zinc followed by a nickel(0)-catalyzed polycondensation reaction. High-molecular-weight polymers featuring reasonable polydispersity can be obtained under suitably controlled reaction conditions.[30] McCullough et al.[32] and Gao et al.[35] performed coupling reactions of the Grignard products formed from 3-alkyl-2-bromothiophene or 3-alkyl-2,5-dibromothiophene to obtain high-molecular-weight regioregular PATs in good yields.

Ymakis and Amaratunga[37] blended poly(3-octylthiophene) as a photoexcitable electron donor with single-walled carbon nanotubes [(SWNTs) nanotube concentration: <1%] as electron acceptors to prepare SWNT/polymer devices that exhibited PV behavior with an open-circuit voltage of 0.7–0.9 V. The short-circuit current (I_{SC}) was 2 orders of magnitude greater than that of the pristine polymer diodes, and the fill factor (FF) also increased from 0.3 to 0.4. The authors proposed that the main reason for this increase was the photoinduced excitons traveling at the polymer–nanotube interface and the SWNTs dissociating the excitons to create continuous percolation paths for the electrons to be transported efficiently to the cathode. A previous study[38] using SWNTs as the interlayer also improved the performance of P3HT-based solar cells. Shao et al.[39] found that an interface layer exhibiting higher crystallinity provided superior solar-cell performance because of the higher charge mobility.

In this study, we synthesized one-dimensional (1D) acid-doped polyaniline nanotubes (a-PANINTs) for use as the interfacial layer in P3HT:[6,6]-phenyl-C$_{61}$-butyric acid methyl ester (PCBM)-based polymer BHJ solar cells to collect holes efficiently from the active layer and transport them to the buffer layer under the internal electric field within fabricated indium tin oxide (ITO)/buffer/a-PANINTs/P3HT:PCBM/Al devices. The use of a-PANINT as an interlayer in these modified devices is attractive for several reasons. The efficiency of photoinduced charge generation depends not only on the quality of the interface with the P3HT/PCBM BHJ interlayer but also on the quality of the interface between the active layer and the a-PANINTs. The extremely high 1D surface area of a-PANINTs can enhance the dissociation of excitons. The extended polyaniline

* Electrochemical Society Active Member.
z E-mail: ykhan@cc.kuas.edu.tw

molecules are arranged helically into nanofibers or nanotubes to prevent intra- or intermolecular complexation and to retain their high conjugation lengths, which provide long pathways for holes to travel without exciton recombination or interference from impurities.[40,41]

Experimental

Characterization.— All reactions were performed under prepurified nitrogen; tetrahydrofuran (THF) and diethyl ether were dried over Na/benzophenone ketyl radical and freshly distilled prior to use. All compounds were characterized from their ^{1}H NMR spectra, which were collected on Unity plus-400, Mercury plus-400, and Varian FT-NMR 400 spectrometers with CDCl$_3$ as solvent and tetramethylsilane as the internal standard. The regioregularity was calculated from the ^{1}H NMR spectra by comparing the relative integrations of the signals at chemical shifts of ca. 2.80 [head-to-tail (*H-T*)] and 2.58 [head-to-head (*H-H*)] ppm. The average molecular weights (M_n and M_w) and PDI of the polymers were determined through gel permeation chromatography (GPC) using a Waters binary HPLC pump, polystyrene standards, and THF as the solvent. Thermogravimetric analysis (TGA) was performed using a TGA/Perkin–Elmer Thermal Analyst Pyris system equipped with a TGA 1 thermogravimetric analyzer and operated at a heating rate of 10°C min^{-1} and a nitrogen flow rate of 20 mL min^{-1}. Differential scanning calorimetry (DSC) was performed using a Pyris Jade DSC/Perkin-Elmer instrument operated at a heating rate of 10°C min^{-1} and a nitrogen flow rate of 40 mL min^{-1}. UV/visual (UV/vis) spectra were recorded on a Perkin-Elmer Lambda 35 UV/vis spectrometer, using solutions prepared from the copolymers dissolved in *o*-xylene or films dip-coated onto quartz from *o*-xylene solution. The surface morphologies of the films were characterized using a BenYuan CSPM 4000 scanning probe microscope and an atomic force microscope (AFM) operated in the tapping mode. To obtain samples for AFM imaging, the thin films were deposited onto slide glass substrates and annealed on a hot plate at 110°C in air for 10 min. The energy level of the highest occupied molecular orbital (HOMO) was obtained through photoelectron spectroscopy in air using a Riken Keiki AC-2 surface analyzer. The energy gap (E_g) was determined from the absorption maximum in the solid state, measured from films spin-coated onto quartz from chloroform (CHCl$_3$) solution. The current-voltage (*I-V*) curves were obtained using a Keithley 2400 source meter and a Newport Oriel 91160 solar simulator system under AM 1.5 illumination (100 mW cm^{-2}). A single-crystalline silicon solar cell was used as a reference cell to confirm the stability of the light source. The mismatch factor was not taken into account. The cell was illuminated from the ITO side. The power conversion efficiency (PCE) of the PV cells was calculated using the following equations

$$PCE = FF \frac{V_{oc} I_{sc}}{P_{in}} \qquad [1]$$

$$FF = \frac{V_{max} I_{max}}{V_{oc} I_{sc}} \qquad [2]$$

where P_{in} is the power of the incident light, V_{oc} is the open-circuit voltage, I_{sc} is the short-circuit current, and V_{max} and I_{max} represent the voltage and current at maximum power.

All reactions (Scheme 1) were performed under dry nitrogen using standard Schlenk techniques and flame-dried vessels. Soxhlet purifications of polymers were performed under dry nitrogen using degassed solvents and nonsolvents. CHCl$_3$ was dried and distilled over CaH$_2$. All materials were purchased from Aldrich. PCBM was purified through column chromatography using *o*-xylene as the eluent (yield: 93%).

Synthesis of a-PANINTs.— A solution of *n*-dodecylbenzene-sulfonic acid [(DBSA), 3 g] and ammonium persulfate (6 g) in deionized (DI) water (30 mL) was mixed with a solution of aniline
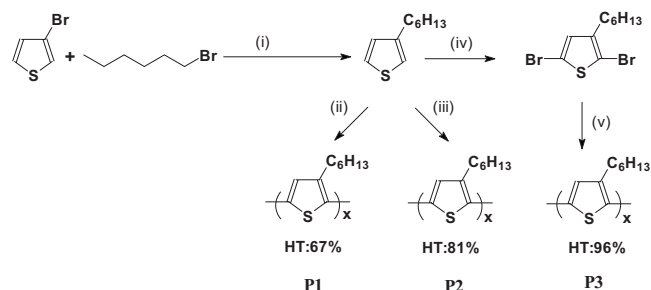
Scheme 1. Synthesis of polymers. Conditions and reagents: (i) 1.1 eq. Mg, Ni(dppp)Cl$_2$, diethyl ether; (ii) 4 eq. FeCl$_3$, anhydrous CHCl$_3$, 25°C; (iii) 4 eq. FeCl$_3$, anhydrous CHCl$_3$, 0°C; (iv) NBS, anhydrous THF, 25°C; and (v) *t*-BuMgCl, Ni(dppp)Cl$_2$, anhydrous THF, 0°C.

(1 g) in HCl (ca. pH 1.5, 5 mL). The resulting dark-green mixture was gently stirred for 5 min and then a further charge of aniline (10 g) was added. After 4 h of gentle magnetic stirring, the green/black precipitate of the a-PANINTs was suction-filtered and washed with copious amounts of DI water and methanol. Drying under vacuum at 100°C for 12 h yielded a dark-green powder. The a-PANINTs were purified through filtration and extraction with methanol in a Soxhlet apparatus for 24 h, followed by drying under vacuum at 50°C for another 24 h (yield: 93%). A portion of this a-PANINT powder (0.5 g) was mixed with toluene (10 mL) and zirconium oxide miniballs in a cell suitable for vibration ballmilling. The cell was vibrated in a ball miller (Retsch MM301) three times for 10 min each time to form a well-dispersed state.

3-Hexylthiophene.— 1-Bromohexane (0.05 mol) was added to a suspension of Mg (0.14 mol) in dry ethyl ether (150 mL). After the complete disappearance of Mg, which was accompanied by a slight increase in temperature, a solution of 3-bromothiophene (0.12 mmol) and [1,3-bis(diphenylphosphino)propane]dichloronickel(II) [Ni(dppp)Cl$_2$, 0.01 mol] in ethyl ether (200 mL) was added. After stirring for 2 h, the reaction mixture was cooled in a crushed-ice bath and 3 N HCl was added. The organic layer was extracted with ethyl ether and dried (MgSO$_4$). After rotary evaporation of the solvent, the residue was distilled (b.p.: 54°C/0.1 Torr) to obtain a colorless liquid (86%). ^{1}H NMR (400 MHz, CDCl$_3$) δ (ppm): 7.227 (s, 1H), 6.915 (s, 1H), 2.618 (*t*, *J* = 7.6 Hz, 2H), 1.613 (m, 2H), 1.305 (m, 6H), 0.893 (m, 3H); ^{13}C NMR (150 MHz, CDCl$_3$) δ (ppm): 139.9, 133.7, 130.5, 128.6, 31.7, 30.5, 29.5, 29.3, 22.6, and 14.6.

2,5-Dibromo-3-hexylthiophene.— *N*-Bromosuccinimide [(NBS), 110 mmol] was added to a solution of 3-hexylthiophene (50 mmol) in dimethylformamide (200 mL), and then the mixture was stirred at room temperature. After 12 h, *n*-hexane was added to precipitate the succinimide, which was filtered off. After rotary evaporation of the solvent, the residue was distilled (b.p. 120°C/0.1 Torr) to obtain as a clear, yellow oil (75%). ^{1}H NMR (400 MHz, CDCl$_3$) δ (ppm): 7.254 (s, 1H), 6.770 (s, 1H), 2.498 (*t*, *J* = 7.6 Hz, 2H), 1.513 (m, 2H), 1.311 (m, 6H), 0.896 (m, 3H). ^{13}C NMR (150 MHz, CDCl$_3$) δ (ppm): 142.8, 128.0, 124.8, 119.6, 31.7, 30.5, 30.2, 29.0, 22.6, and 14.7.

Preparation of poly(3-hexylthiophene)s at 25°C (P1) and 0°C (P2).— 3-Hexylthiophene was added to a suspension of anhydrous FeCl$_3$ (40 mmol) in anhydrous CHCl$_3$ (400 mL), and then the mixture was stirred at 25°C. After 7 h, the reaction mixture was poured into methanol (500 mL) and the resulting red-black precipitate was filtered. The precipitate was purified with methanol in a Soxhlet apparatus for 72 h. The brown precipitate was filtered off and dried in a vacuum oven to yield the polymer P1 as a dark-brown solid (35%). ^{1}H NMR (400 MHz, CDCl$_3$) δ (ppm): 6.98 (s, 1H), 2.80 (s,

Table I. Physical properties of the P3HTs.

Polymer	H–T[a] (%)	M_n[b]	M_w[b]	PDI[b]	T_d[c] (°C)	T_m[d] (°C)	E_g[e] (eV)	HOMO[f] (eV)	LUMO[g] (eV)
P1	67	26,700	45,000	1.68	433	160	1.97	−4.93	−2.96
P2	81	48,000	66,000	1.37	451	185	1.94	−4.93	−2.99
P3	96	29,800	37,000	1.24	459	220	1.91	−4.91	−3.00

[a] Regioregularity calculated from ^{1}H NMR spectrum, comparing the relative integrals of the signals at chemical shifts of ca. 2.80 (H–T) and 2.58 (H–H) ppm.
[b] Molecular weights (M_n and M_w) and PDI determined using GPC with THF as the solvent (calibration with narrowly distributed polystyrene standards).
[c] Temperature of 5% weight loss determined using TGA.
[d] Melting point under N_2 determined through DSC at a heating rate of 10°C min^{-1} from −40 to + 300°C.
[e] Optical bandgap determined from the value of λ_{onset} in UV/vis spectra.
[f] HOMO energy level measured using a Riken Keiki AC-2 surface analyzer.
[g] LUMO energy level calculated according to the equation $E_{LUMO} = E_{HOMO} + E_g$.

2H), 2.58 (*t*, *J* = 7.5 Hz, 2H), 1.71 (m, 2H), 1.34 (m, 6H), and 0.90 (m, 3H). P2 was prepared using the same procedure, but at a reaction temperature of 0°C. Its ^{1}H NMR spectrum (400 MHz, CDCl$_3$) was identical to that of P1.[42]

Preparation of the highly regioregular poly(3-hexylthiophene) P3.— A dry three-necked flask was charged with 2,5-dibromo-3-hexylthiophene (500 mg, 1.5 mmol) and anhydrous THF (30 mL). A solution of *tert*-butylmagnesium chloride (2 M, 1 mL, 2 mmol) in diethyl ether was added via a purged syringe, and then the reaction mixture was heated under a gentle reflux for 2 h. After cooling to room temperature, Ni(dppp)Cl$_2$ (26 mg, 0.046 mmol) was added to the reaction mixture. The polymerization was left to proceed under stirring for 24 h at 0°C and then the mixture was quenched with 5 M HCl. The reaction mixture was then concentrated through rotary evaporation and the precipitate filtered and dried under vacuum at 50°C for 24 h.

The three polymers, P1, P2, and P3, were purified through a series of sequential Soxhlet extractions with methanol, hexane, and CHCl$_3$. The fractionation process was performed to diminish the effect from short polymers on the PV performance of the cells and to lower the PDI of each polymer. The fractionation process was performed using a procedure described previously;[43] the properties of the polymers are summarized in Table I. The fractional precipitations of P1 and P2 were performed by adding methanol to the supernatants and cooling them into *o*-xylene at 0°C for 24 h. The precipitates was collected through centrifugation at 25°C.

Device fabrication.— Poly(3, 4-ethylenedioxythiophene : poly (styrenesulfonate) (PEDOT-PSS, Baytron AI 4083) was spin-coated from an aqueous solution onto precleaned ITO-coated glass (sheet resistance: 15 Ω/□; Ritek) at a thickness of 30 nm, and then the substrate was dried at 150°C for 10 min. The a-PANINT layer (40–50 nm) was then deposited onto the PEDOT-PSS layer through spin-coating from a toluene solution (0.2 mg mL^{-1}, 5 mL). Next, a 1:1 (w/w) mixture of P3HT and PCBM (100 mg mL^{-1}) in *o*-xylene was deposited through dip-coating (2 cm min^{-1}) without any filtration under an inert atmosphere onto the a-PANINT layer, and then the sample was dried at 150°C for 10 min. Finally, the Al electrode (150 nm) was deposited on top of the active layer by thermal evaporation at ca. 2 × 10^{-6} Torr through a mask defining the active area of the device as 3 mm^2. Thermal annealing was performed by heating the devices on a calibrated hot plate at 120°C for 20 min under a nitrogen atmosphere.

Results and Discussion

Figure 1 displays field-emission scanning electron microscopy (SEM), transmission electron microscopy (TEM), and X-ray diffraction (XRD) images of the a-PANINTs. The SEM image reveals that the product comprised >10 μm long tubes having a mean diameter in the range of 200–300 nm, which decreased to ca. 50–70 nm after removing complexed DBSA using ammonia water (neutralization). The TEM image indicates that each a-PANINT existed in the form of a well-extended 1D nanostructure, which could aid in the transport of charges further through the tubular structure, thereby preventing interference, recombination with electrons, or defects. We did not, however, detect the hollow tubular structure for the emeraldine base dedoped-type PANINTs because the tubes shrank into solid nanofibrous/dendritelike morphologies as a result of strong intermolecular hydrogen bonding after the complexed DBSA was removed entirely. The electrical conductivity (σ_{RT}) of the a-PANINT compressed pellet was in the range of 3–4 S cm^{-1}, higher than the average conductivity of common PANIs, which are mostly <1 S cm^{-1} and, in some cases, reach as low as 0.1 S cm^{-1}. We assign the peaks in the XRD pattern in Fig. 1c at 3, 20, and 27° to the periodic distance between the dopant and the nitrogen atoms on adjacent main chains and to the periodicities parallel and perpendicular to the polymer chains, respectively. Our results indicate that the a-PANINT layer was partly crystalline as a result of its special tubular morphology, which was further enhanced after thermal treatment. We expected that the crystalline, submicron-scale, well-extended 1D nanostructural features on the a-PANINT surface would be an appropriate match for the P3HT/PCBM thermally agi-
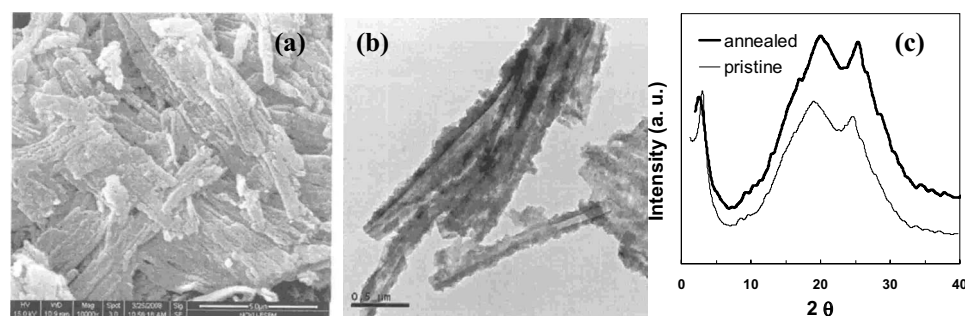
Figure 1. (a) SEM, (b) TEM, and (c) XRD images of a-PANINTs.
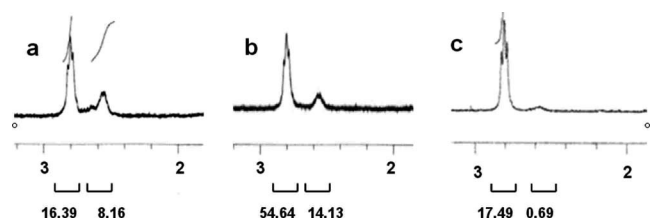
Figure 2. ^{1}H NMR spectra of P3HTs possessing H–T regioregularities of (a) 67, (b) 81, and (c) 96%.

tated crystalline domain, providing a well-defined contact area for the transport of free charge carriers and, correspondingly, improved device performance.

The ^{1}H NMR spectra in Fig. 2 display the signals assigned to the α-methylene protons of the three P3HT polymers; they can be resolved into H–T and H–H dyads. The chemical shifts of the α-methylene protons in the H–T and H–H systems appeared at 2.80 and 2.58 ppm, respectively. As the regioregularity increased, the intensity of the H–T peak increased relative to that of the H–H signal. Relative integration of the H–T and H–H peaks provided percentage regioregularities (H–T coupling contents) for P1, P2, and P3 of 67, 81, and 96%, respectively.

P1, P2, and P3 were dissolved separately in *o*-xylene (1 wt %) at 90°C and then cooled to room temperature and left for 24 h. Figure 3 displays the UV/vis absorption spectra of these solutions. It is interesting that all three of these P3HTs formed gel-ordered structures after heating to 90°C and then cooling slowly to ambient temperature. The regioregularities of the three P3HTs had an effect on the time required to obtain the gel-ordered behavior. The maximum absorption bands in the UV/vis spectra of P1, P2, and P3 were positioned at 450 nm. After cooling from 90°C to ambient temperature for 1 h, low-energy shoulders appeared at 605 nm for the three different-regioregularity polymer solutions, revealing the formation of ordered, microcrystalline P3HT domains having a coplanar intrachain conformation. For P1, additional low-energy shoulders at 560 and 605 nm began to increase in intensity after 24 h; for both P2 and P3, the shoulders appeared at 510, 560, and 605 nm. These phenomena reveal that the structure possessing higher regioregularity formed highly ordered, microcrystalline lamella domains after a certain amount of time.[44] The P3HT solution prepared using
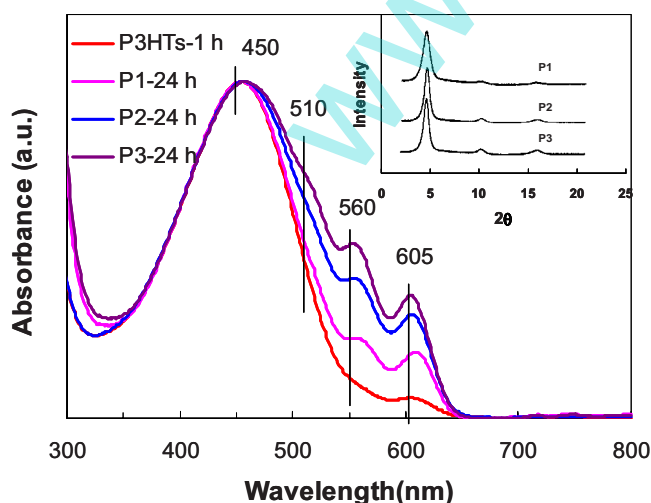
p-xylene[45] as a solvent required a longer time to reach its steady state of gelation, indicating that the solvent plays a key role during the aggregation of conjugated polymers and the optoelectronic performance in the solid state. We attribute the shoulders at 550 and 605 nm to chiral exciton coupling of chirally stacked and chirally aligned polymer strands, respectively.[46] Therefore, the UV/vis spectra revealed that the structures we obtained were composed of highly ordered polymer chains. The increases in intensity of the absorbances at 510, 550, and 605 nm after 24 h indicate that the kinetic processes that were in effect required time to reach the equilibrium rod concentration.[47,48] An increase in the conjugation length of P3HTs causes low-energy shoulders to appear in UV/vis spectra, arising from π–π* interchain overlapping.[49] We conclude that our P3HTs having higher degrees of regioregularity featured higher concentrations of their coplanar intrachain overlapping conformation after heating to 90°C and cooling to ambient temperature to form the gelation phase. We suspected that this highly ordered nanorod surface might interact well with the surface of the a-PANINT layer. The inset to Fig. 3 displays XRD patterns of the thin films of the three P3HTs deposited through dip-coating; the peaks represent the distances between the polymer main chains ($2\theta = 5°$), the periodicities parallel to the polymer chains ($2\theta = 10.5°$), and the distances between overlapping thiophene rings ($2\theta = 17°$).[50] Thus, the dip-coating process provided films exhibiting highly crystalline structures, with the higher-regioregularity polymer having the highest degree of crystallinity. We expect that these highly ordered nanorod structures might interact well with the surfaces of the a-PANINT films. We prepared the active layer from the sol–gel solution by heating a mixture of P3HT and PCBM (1:1, w/w) in *o*-xylene at

Figure 3. (Color online) UV/vis absorption spectra of P1, P2, and P3 (1 wt %) in *o*-xylene solutions. The mixtures were heated at 90°C to completely dissolve the polymers and then cooled to room temperature and left to stand for 24 h.
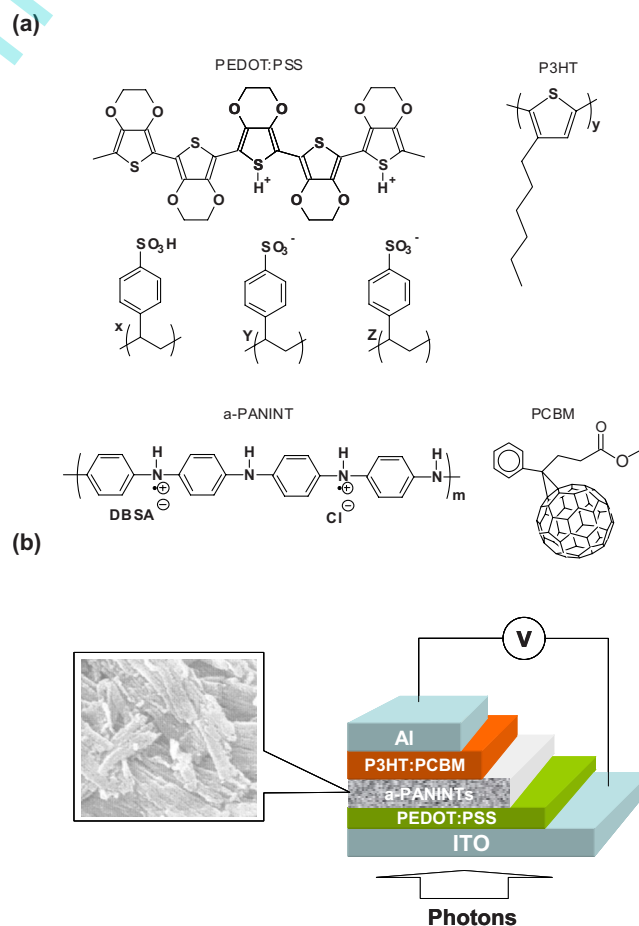
Scheme 2. (a) Chemical structures of the materials used in the devices. (b) Device structure.
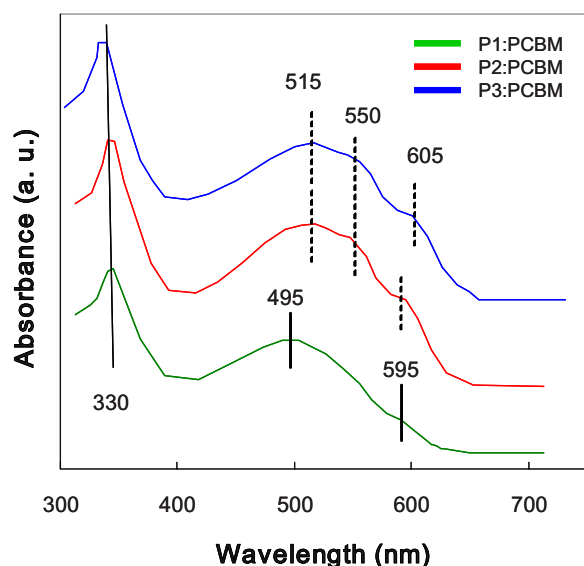
Figure 4. (Color online) UV/vis spectra of P3HT/PCBM (1:1 wt %) films.

90°C and then cooling slowly to ambient temperature. After 24 h, the active layer was dip-coated onto the a-PANINT layer and then the system was dried at 150°C for 10 min. Scheme 2 presents the chemical structures of the materials employed and the device architecture.

Figure 4 displays the UV/vis spectra of the P3HT:PCBM blended films. The UV/vis absorption bands of the P1:PCBM solid film appeared at 495 and 595 nm; for the P2:PCBM blended solid film, they were positioned at 515, 550, and 595 nm. Those of the P3:PCBM blended solid film were centered at 515, 550, and 605 nm. Thus, when the regioregularity of the P3HT increased from 67% to 81 or 96%, the maximum absorption band shifted from 495 to 515 nm, revealing a greater degree of $\pi-\pi^*$ interchain overlap in the solid state. It is interesting that the UV/vis absorption band at 550 nm was absent for the P1:PCBM film, but present for those of P2 and P3. This behavior might suggest that the "short range" conjugation length was broken by introducing the PCBM nanoparticles into the low-regularity P1 aggregation phase, whereas the "long-range" conjugation lengths of P2 and P3 remained at 550 nm. When the regioregularity of the P3HT increased from 67 to 96%, the band at 595 nm shifted to 605 nm, indicating that the higher regioregularity improved the degree of coplanar $\pi-\pi$ interchain overlap and increased the conjugation length in the solid state (i.e., the H–T structure of hexylthiophene units determines both the interchain overlap and the length of conjugation). This aggregation and gelation mechanism has been discussed in detail previously.[51] We expected the long conjugation length of P3HT or a-PANINT to aid the transformation of free carriers and improve the PV performance in our fabricated devices.[45,52]

Figure 5 displays AFM images of the P3HT/PCBM blended solid films after dip-coating and annealing. For the P1:PCBM solid film, we observe large-scale phase separation ($>$100 nm), which is not favorable for charge separation, charge transport, or charge collection.[8] The P2:PCBM and P3:PCBM films possess smaller domains ($<$100 nm) (i.e., smaller-scale phase separation), which we expected would provide higher-quality BHJ interfaces for exciton generation and charge formation. During annealing at 150°C for 30 min, the conformation of P3HT changes to form lamellar structures exhibiting improved $\pi-\pi$ stacking; simultaneously, the PCBM and P3HT components demix and the morphology self-assembles into a BHJ material that is optimum for PV performance.[43]

Figure 6 presents *I-V* curves of the devices we fabricated with and without a-PANIN interfacial layers; Table II summarizes their PV performance. The PCEs of devices D1, D3, and D5, which lacked a-PANINT layers, were 0.97, 1.36, and 2.17%, respectively,
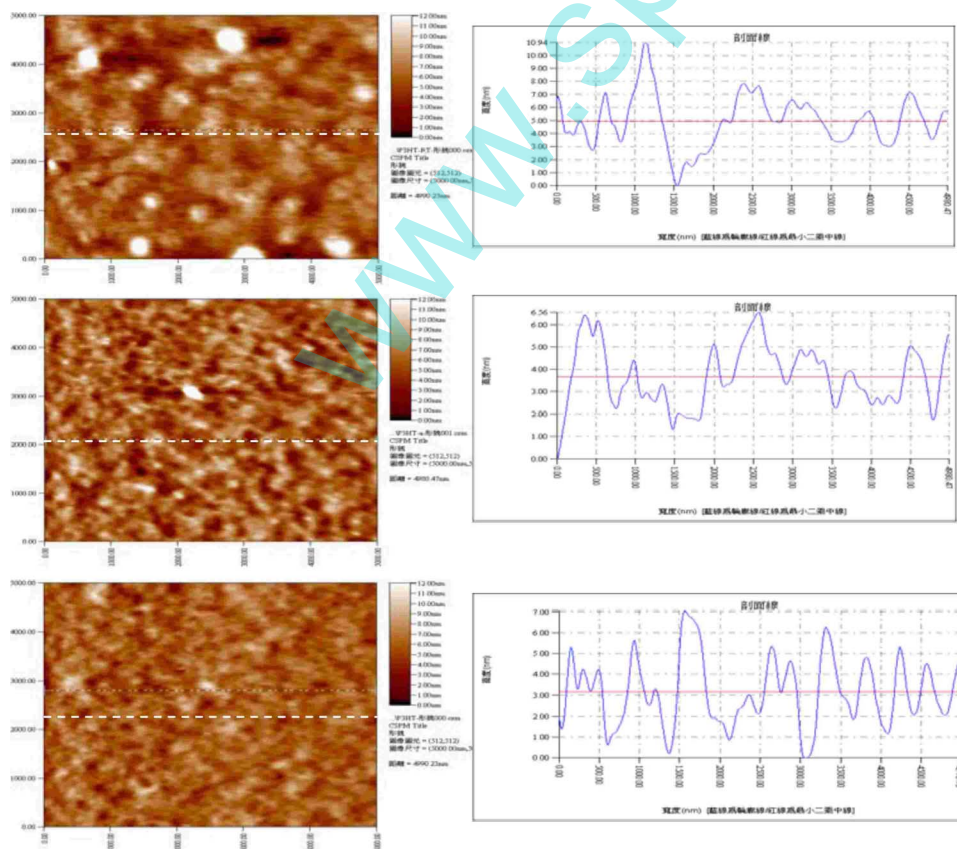
Figure 5. (Color online) AFM images of P3HT/PCBM blended films.
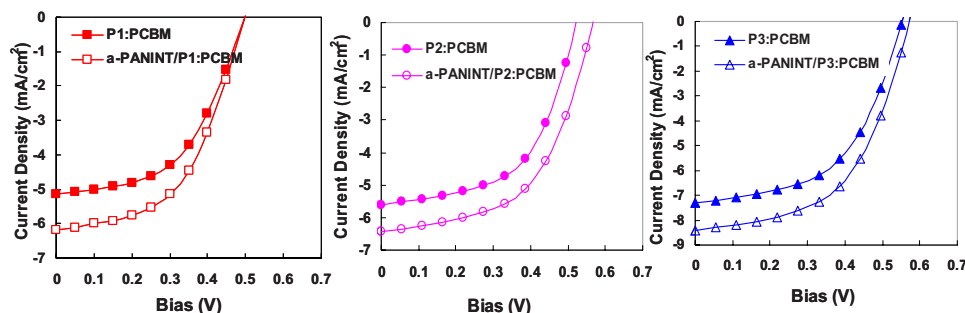
Figure 6. (Color online) *I-V* characteristics (AM 1.5 G, 100 mW cm^{-2}) of devices D1–D6.

indicating that the higher-regioregularity polymer structures possessed a higher degree of internal coplanar overlap and a longer conjugation length for carrier transport under the internal electrical field. It appears that the more symmetrical chain sequence in D5 provided better packing in the solid state, leading to a slightly longer effective conjugation length. Clearly, structural regioregularity plays an important role in enhancing PV performance, especially in the BHJ structures of solar cells. Thus, for devices prepared without a-PANINT layers, the regioregularity of the polymer structure determines the photon absorption, exciton separation, and carrier transportation in the active layer.

The devices D2, D4, and D6, which incorporated a-PANINT layers, exhibited higher PCEs and PV performances than did their corresponding a-PANINT-free devices. These findings suggest that the 1D tubular morphology of the a-PANINT layer provided a well-defined contact surface, efficient pathways for the transportation of free charge carriers toward their respective electrodes, and a reduced number of cul de sacs for holes, thereby reducing the degree of exciton recombination within the photoactive cells and increasing their PV performance.

For P3HT-based devices featuring ohmic contacts at both electrodes, the value of V_{OC} varies linearly with the energy difference between the donor's HOMO and the acceptor's lowest unoccupied molecular orbital (LUMO), unless splitting of the LUMO/HOMO levels occurs as a result of strong interchain or interlayer interactions originating from relatively high ordering of the P3HT. The value of V_{OC} of our cells remained at ca. 0.51–0.57 V; the slight variation resulted presumably from measurement errors arising from the equipment used. Thus, the value of V_{OC} of a-PANIN/P3HT:PCBM-based solar cells is not affected by the incorporation of a-PANINT as an interfacial layer, but it is affected by the thermal treatment process.[39]

The HOMO energy levels of the a-PANINT films were identical (5.1 eV); i.e., the incorporation of a-PANINT had no observable effect on the value of V_{OC} of the cells. The constant value of V_{OC} among the various systems suggests equal energy differences be-

tween the HOMO of the active layer and the HOMO of the a-PANINT layer. The a-PANINT-modified films exhibited higher values of I_{SC}, with the maximum value of 8.43 mA cm^{-2} obtained for device D6. The FFs also increased for the a-PANINT-modified devices. As a result, the maximum PCE of the cell (2.78%) occurred when the H–T content was 96%; the corresponding values of I_{SC}, V_{OC}, and FF were 8.43 mA cm^{-2}, 0.57 V, and 0.58, respectively. This PCE is a 28% improvement over that of the unmodified cell.

We propose the following PV mechanisms for the functioning of the solar cells incorporating the a-PANIN interfacial layers: (*i*) The bulk heterojunction P3HT:PCBM photoactive layer accepts photons from white light and generates excitons. (*ii*) The partial excitons are swept to the well-contacted, highly ordered a-PANIN interfacial layer under the influence of the built-in chemical and electric potentials. The high conductivity and mobility of the annealed a-PANIN layer efficiently extracts the photo-induced holes, providing conducting pathways to the buffer layer while reducing the degree of exciton recombination and resulting in a more efficient charge separation. The enhanced hole collection can be ascribed in part to geometrical field enhancement at the a-PANIN layer. The greater order in the structure of the a-PANINs following thermal treatment improved the degree of contact between the buffer layer and the photoactive film, decreasing the series resistance of the cell while increasing both the current and the FF. (*iii*) The separated free charge carriers proceed toward their respective electrodes.

Conclusion

Using FeCl$_3$ as an oxidant and the Grignard metathesis (McCullough) method, we have synthesized three P3HTs (P1–3) exhibiting different structural regioregularities. From ^{1}H NMR spectra, we determined that the regioregularities (H–T coupling contents) of P1, P2, and P3 were 67, 81, and 96%, respectively. UV/vis spectra revealed that these P3HTs formed highly ordered structures in *o*-xylene after heating at 90°C and then cooling to ambient temperature and standing for 24 h. The PV performance of devices fabricated without a-PANINT as an interfacial layer increased as the regioregularity of P3HT increased. The PCEs of the devices incorporating the a-PANINT interfacial layer were higher than those of the corresponding a-PANINT-free devices. This behavior suggests that the high conductivity and controlled tubular nanoscale morphology of the annealed a-PANINT layer resulted in efficient extraction of photogenerated holes to the buffer layer and suppression of exciton recombination, thereby improving the PV performance. Thus, the performance of solar cells can be improved significantly after incorporating an a-PANINT layer into the device structure, without complicating the device fabrication process.

Acknowledgment

Table II. Performance characteristics of PV cells measured under AM 1.5 G, 100 mW cm^{-2} solar illumination.

Device[a]	Layer	V_{oc} (V)[b]	I_{sc} (mA cm^{-2})[c]	FF (a.u.)[d]	PCE (%)[e]
D1	P1:PCBM	0.51	5.15	0.38	0.97
D2	a-PANINT/P1:PCBM	0.51	6.18	0.39	1.20
D3	P2:PCBM	0.52	5.6	0.47	1.36
D4	a-PANINT/P2:PCBM	0.56	6.4	0.47	1.72
D5	P3:PCBM	0.56	7.33	0.53	2.17
D6	a-PANINT/P3:PCBM	0.57	8.43	0.58	2.78

[a] Device configuration: ITO/PEDOT:PSS/Layer/Al.
[b] Open-circuit voltage.
[c] Short-circuit current.
[d] Fill factor.
[e] Power conversion efficiency.

References

1. I. Schwendeman, R. Hickman, G. Sonmez, P. Schottland, K. Zong, D. M. Welsh,

and J. R. Reynolds, *Chem. Mater.*, **14**, 3118 (2002).
2. R. Singhal, A. Chaubey, K. Kaneto, W. Takashima, and B. D. Malhotra, *Biotechnol. Bioeng.*, **85**, 277 (2003).
3. D. Villers, D. Jobin, C. Soucy, D. Cossement, R. Chahine, L. Breau, and D. Belanger, *J. Electrochem. Soc.*, **150**, A747 (2003).
4. T. Tuken, B. Yazici, and M. Erbil, *Prog. Org. Coat.*, **51**, 205 (2004).
5. Z. Bao, A. Dodabalapur, and A. J. Lovinger, *Appl. Phys. Lett.*, **69**, 4108 (1996).
6. S. H. Ahn, M. Czae, E. R. Kim, H. Lee, S. H. Han, J. Noh, and M. Hara, *Macromolecules*, **34**, 2522 (2001).
7. F. Padinger, R. S. Rittberger, and N. S. Sariciftci, *Adv. Funct. Mater.*, **13**, 85 (2003).
8. Y. Kim, S. Cook, S. A. Choulis, J. Nelson, J. R. Durrant, and D. D. C. Bradley, *Chem. Mater.*, **16**, 4812 (2004).
9. A. Gadisa, M. Svensson, M. R. Andersson, and O. Inganas, *Appl. Phys. Lett.*, **84**, 1609 (2004).
10. W. L. Ma, C. Y. Yang, X. Gong, K. Lee, and A. J. Heeger, *Adv. Funct. Mater.*, **15**, 1617 (2005).
11. G. Li, V. Shrotriya, Y. Yao, and Y. Yang, *J. Appl. Phys.*, **98**, 043704 (2005).
12. S. S. Zade and M. Bendikov, *J. Org. Chem.*, **71**, 2972 (2006).
13. A. M. Ballantyne, L. Chen, J. Dane, T. Hammant, F. M. Braun, M. Heeney, W. Duffy, I. McCulloch, D. D. C. Bradley, and J. Nelson, *Adv. Funct. Mater.*, **18**, 1 (2008).
14. S. S. Pandey, W. Takashima, S. Nagamatsu, T. Endo, M. Rikukawa, and K. Kaneto, *Jpn. J. Appl. Phys., Part 2*, **39**, 94 (2000).
15. T. Otsubo, Y. Aso, K. Takimiya, H. Nakanishi, and N. Sumi, *Synth. Met.*, **133**, 325 (2003).
16. R. J. Kline, M. D. McGehee, E. N. Kadnikova, J. Liu, J. M. J. Fréchet, and M. F. Toney, *Macromolecules*, **38**, 3312 (2005).
17. M. Leclerc, F. M. Diaz, and G. Wegner, *Makromol. Chem.*, **190**, 3105 (1989).
18. R. Sugimoto, S. Takada, H. B. Gu, and K. Yoshino, *Chem. Express*, **1**, 635 (1986).
19. K. Tamoa, K. Sumitani, and M. Kumada, *J. Am. Chem. Soc.*, **94**, 4376 (1972).
20. K. Tamao, K. Sumitani, Y. Kiso, M. Zembayashi, A. Fujioka, S. Kodama, I. Nakajima, A. Minato, and M. Kumada, *Bull. Chem. Soc. Jpn.*, **49**, 1958 (1976).
21. T. Yamamoto, K. Sanechika, and A. Yamamoto, *J. Polym. Sci., Polym. Lett. Ed.*, **18**, 9 (1980).
22. T. Yamamoto, A. Morita, Y. Miyazaki, T. Maruyama, H. Wakayama, Z. H. Zhou, Y. Nakamura, T. Kanbara, S. Sasaki, and K. Kubota, *Macromolecules*, **25**, 1214 (1992).
23. T. Yamamoto, K. Osakada, T. Wakabayashi, and A. Yamamoto, *Makromol. Chem., Rapid Commun.*, **6**, 671 (1985).
24. T. Yamamoto, T. Maruyama, Z. H. Zhou, Y. Miyazaki, T. Kanbara, and K. Saneckika, *Synth. Met.*, **41**, 345 (1991).
25. J. K. Stille, *Angew. Chem., Int. Ed. Engl.*, **25**, 508 (1986).
26. S. Kodama, I. Naajima, M. Kumada, A. Minato, and K. Suzuki, *Tetrahedron*, **38**, 3347 (1982).

27. T. A. Chen and R. D. Rieke, *Synth. Met.*, **60**, 175 (1993).
28. T. A. Chen and R. D. Rieke, *J. Am. Chem. Soc.*, **114**, 10087 (1992).
29. T. A. Chen, R. A. O'Brien, and R. D. Rieke, *Macromolecules*, **26**, 3462 (1993).
30. T. A. Chen, X. Wu, and R. D. Rieke, *J. Am. Chem. Soc.*, **117**, 233 (1995).
31. X. Wu, T. A. Chen, and R. D. Rieke, *Macromolecules*, **28**, 2101 (1995).
32. R. D. McCullough, R. D. Lowe, M. Jayaraman, and D. L. Anderson, *J. Org. Chem.*, **58**, 904 (1993).
33. R. S. Loewe, S. M. Khersonsky, and R. D. McCullough, *Adv. Mater. (Weinheim, Ger.)*, **11**, 250 (1999).
34. R. Miyakoshi, A. Yokoyama, and T. Yokozawa, *Macromol. Rapid Commun.*, **25**, 1663 (2004).
35. Z. Gao, K. S. Siow, and H. S. O. Chan, *Synth. Met.*, **75**, 5 (1995).
36. R. Singh, J. Kumar, R. K. Singh, A. Kaur, K. N. Sood, and R. C. Rastogi, *Polymer*, **46**, 9126 (2005).
37. E. K. Ymakis and G. A. J. Amaratunga, *Appl. Phys. Lett.*, **80**, 112 (2002).
38. S. Chaudhary, H. Lu, A. M. Muller, C. J. Bardeen, and M. Ozkan, *Nano Lett.*, **7**, 1973 (2007).
39. Y. Shao, S. Sista, C. W. Chu, D. Sievers, and Y. Yang, *Appl. Phys. Lett.*, **90**, 103501 (2007).
40. B. Z. Hsieh, H. Y. Chuang, L. Chao, Y. J. Li, Y. J. Huang, P. H. Tseng, T. H. Hsieh, and K. S. Ho, *Polymer*, **49**, 4218 (2008).
41. M. Y. Chang, C. S. Wu, I. F. Chen, B. Z. Hsieh, W. Y. Huang, K. S. Ho, T. H. Hsieh, and Y. K. Han, *Org. Electron.*, **9**, 1136 (2008).
42. S. Amou, O. Haba, K. Shirato, T. Hayakawa, M. Ueda, K. Takeuchi, and M. Asai, *J. Polym. Sci., Part A: Polym. Chem.*, **37**, 1943 (1999).
43. Y. L. Lu, W. Liu, K. Oshima, T. Yamauchi, M. Shimomura, and S. Miyaichi, *J. Appl. Polym. Sci.*, **77**, 3069 (2000).
44. W. Ma, C. Yang, X. Gong, K. Lee, and A. J. Heeger, *Adv. Funct. Mater.*, **15**, 1617 (2005).
45. S. Berson, R. D. Bettignies, S. Bailly, and S. Guillerez, *Adv. Funct. Mater.*, **17**, 1377 (2007).
46. S. Vandeleene, K. V. den Bergh, T. Verbiest, and G. Koeckelberghs, *Macromolecules*, **41**, 5123 (2008).
47. S. Malik, T. Jana, and A. K. Nandi, *Macromolecules*, **34**, 275 (2001).
48. S. D. D. V. Rughoopath, S. Hotta, A. J. Heeger, and F. J. Wudl, *J. Polym. Sci., Part B: Polym. Phys.*, **25**, 1071 (1987).
49. M. Al-Ibrahim, O. Ambacher, S. Sensfuss, and G. Gobsch, *Appl. Phys. Lett.*, **86**, 201120 (2005).
50. D. H. Kim, Y. D. Park, Y. Jang, S. Kim, and K. Cho, *Macromol. Rapid Commun.*, **26**, 834 (2005).
51. W. Y. Huang, P. T. Huang, Y. K. Han, C. C. Lee, T. L. Hsieh, and M. Y. Chang, *Macromolecules*, **41**, 7485 (2008).
52. R. C. Hiorns, R. D. Bettignies, J. Leroy, S. Bailly, M. Firon, C. Sentein, A. Khoukh, H. Preud'homme, and C. D. Lartigau, *Adv. Funct. Mater.*, **16**, 2263 (2006).